Range-Based Subsea Vehicle Localization: A Measure of Observability

K Kalyan Kumar[1,] Saleha Tabasum[2] P Durga Prasad [3],N Siddhik [4]

[1,2,3,4] Asst. Professor, Department of EEE, K. S. R. M College of Engineering(A), Kadapa

Abstract:

In this research, we focus on the more general issue of single and multiple AUV localization using range measurements, and we examine the accompanying observability problems. Underwater, localization tools like Global Navigation Satellite Systems are ineffective due to attenuation of electromagnetic radiation. Due to the large amount of error introduced by sensor bias and drift, dead reckoning techniques and low-cost motion sensor units are not suitable for AUV localization. To perform trilateration algorithms for determining the distance between an AUV and a fixed network of transponders, localization systems often use acoustic sensors. Costing a lot of money and taking a long time to calibrate, these methods can only pinpoint AUVs within the region specified by the geometry of the transponders. In recent years, a practical alternative to using just the distance between the AUV and a single transponder has evolved. This method uses data from the AUV's on-board motion sensors, such as depth, velocity, and acceleration measurements. The concept might be developed further such that sound sensors are used to calculate the distance between two AUVs. This paper draws inspiration from these developments to show how the same mathematical framework can be used to solve the problems of absolute localization of a single vehicle and relative localization of multiple vehicles, and to modify concepts of observability derived for nonlinear systems to analyze how localization performance varies with the types of motion imparted to the AUVs. Through modeling and practical experiments with a genuine marine vehicle, we show that the performance of an Extended Kalman filter may be improved by using our proposed observability measure for this effect. The filter observer status changes depending on the driving conditions.

Key words :

Keywords include things like "range-only localization," "observability metric," and "submersible.".

Introduction

Autonomous underwater vehicles (AUVs) have gained popularity in recent decades and are currently used extensively in a broad range of fields, from the military and academics to business and commerce. Autonomous underwater vehicles (AUVs) have several potential applications, one of which is assisting marine scientists in carrying out oceanographic environmental monitoring. In order to complete their missions autonomously, AUVs need to be able to precisely locate their position. However, it is well-known that localization systems like Global Navigation Satellite Systems (GNSSs) are ineffective underwater due to the attenuation of electromagnetic radiation, therefore their employment is restricted to short times while the vehicles are above water. In order to determine an AUV's position, inertial and velocity data must be appropriately integrated, which is where dead reckoning comes in. But because of numerical drift caused by the

Dead reckoning is only useful for short dives since it incorporates sensor noise, sensor bias and drift, and is potentially vulnerable to the existence of external currents and model errors. The AUV may need to come to the surface often to update its GNSS position. Another common technique for underwater localization is the use of auditory devices to determine distances between places and/or to estimate the bearing and elevation of a spot with respect to another using auditory signals.

Long Baseline, Short Baseline, and Ultra-Short Baseline systems are examples of commercially available solutions that have seen extensive application for difficult jobs. Long Baseline (LBL) acoustic localization systems use transponders deployed at a set depth and at regular intervals below the surface. The AUV sends out queries to the transponders and measures the time it takes for the reflected acoustic waves to return to its receiver to determine the distance. The trilateration approach is then used to pinpoint the position of the AUV. In Short Baseline (SBL) systems, tens of meters separate the aforementioned transducers that are deployed on a surface vessel. Triangulating the position of the submerged AUV is the responsibility of the surface section, which does so by sending out queries to a transponder installed there. Ultra-short Baseline (USBL) systems use a compact, self-contained device located on a support vessel to estimate the position of an autonomous underwater vehicle (AUV) by measuring the relative phases of the signals supplied to them by the surface segment. The latter two options include feeding back the AUV's projected position. Recently, a new approach has evolved to AUV localization that employs a single transponder (beacon) and transducer to reduce complexity without increasing the cost of sensors.

The AUV may calculate its position using this approach instead of receiving data from a single transponder at a fixed place. An array of additional sensors, such as a depth sensor, a Doppler log, and an inertial measurement unit, are used by the AUV instead. Recent publications [1-4] illustrate the increasing attention paid to this localization issue, which goes by a few other names: single beacon localization, range-only localization, and so on. This paper proposes an observability metric relevant to the single beacon localization problem by using the local weak observability properties of a chosen non-linear system. Therefore, and also for the sake of completeness and clarity, we present a brief summary of important past work in the literature that addresses the aforementioned challenges.

Modelling the Observability of Systems

The issue of relative localisation between two AUVs is first addressed. Let I be an inertial, earth-fixed reference frame specified by the North East Down (NED) convention, and let v,i be a frame with its origin fixed at the centroid of the i-th vehicle (i = 1, 2) and parallel to I (see Figure 1). Hereinafter, we will refer to the inertial velocities of vehicles 1 and 2 as vv,1 = dxv,1/dt and vv,2 = dxv,2/dt, and the positions of vehicles 1 and 2 as xv,1 IR3 and xv,2 IR3, respectively. We denote the system state as x = xv,2xv,1 and the relative velocity of the cars as v = vv,2vv,1. We suppose that it is feasible to gauge not only the separation between vehicles but also their relative velocities and depths using inertial sensors. Here's the notation for a first-order kinematic model of the vehicles' relative motion:

where x represents the current state, v represents the input, and y IR2 is the observable output vector, which is a function, h1, of the Euclidean distance, kaki, and the depth difference, x3, between the two vehicles.

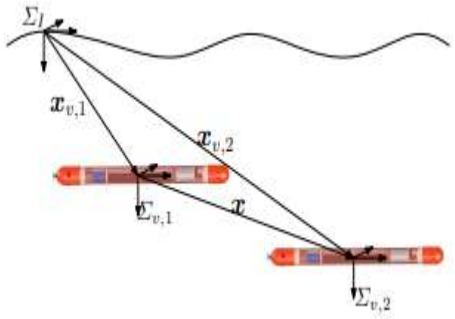

Figure 1. Reference systems: ΣI is the inertial, earth-fixed frame and Σv,i are the moving frame with the origin fixed in the i-th vehicle (i = 1, 2).

In the literature, the range-based localization problem is usually studied in 2D. Here, we start by explicitly including a third dimension (depth) to fully capture manoeuvres that include diving. Once we have shown that the vertical component does not affect the observability of the system, we then move on to the 2D case. Notice also that, since the above model is defined in terms of relative motions, it captures the kinematics of both single beacons, as well as relative multi-vehicle localization problems. To discuss the observability properties of the system in Equation (1), we first recall some basic observability concepts for non-linear systems, summarize important local weak observability properties and describe an observability rank condition; we then apply the latter condition to our specific case.

Single Beacon Localization:

Numerical Simulations This section presents the results of numerical simulations that illustrate the effectiveness of the observability index proposed in assessing the performance that can be obtained with a single beacon localization algorithm. Specifically, we consider a single-beacon localization algorithm that is obtained by implementing an Extended Kalman Filter for a discrete-time version of Equation (5), and we evaluate its performance under different operational conditions (e.g., different vehicle speeds and trajectories) in light of the proposed metric. The system state equation is assumed as:

$$\begin{cases} \boldsymbol{x}_{k+1} &= \boldsymbol{x}_k + T\boldsymbol{v}_k + \boldsymbol{w}_k \\ y_{k+1} &= \frac{1}{2}\boldsymbol{x}_k^{\mathrm{T}}\boldsymbol{x}_k + \mu_k \end{cases}$$

where wk and µk are process and measurement noises, assumed as zero-mean Gaussian noise with

$$\boldsymbol{w}_k \sim \mathcal{N}(0, \boldsymbol{R}_w) \text{ and } \mu_k \sim \mathcal{N}(0, \boldsymbol{R}_\mu); \mathrm{T}$$

is the sample time. An EKF filter for Equation (16) was implemented using the following standard equations: (1) Time update of state and estimation error covariance:

$$\begin{aligned} \hat{\boldsymbol{x}}_{k+1}^{-} &= \hat{\boldsymbol{x}}_k^{+} + T\boldsymbol{v}_k \\ \boldsymbol{P}_{k+1}^{-} &= \boldsymbol{P}_k^{+} + \boldsymbol{R}_w \end{aligned}$$

(2) Measurement updates of state and estimation error covariance:

$$\begin{aligned} K_{k+1} &= P_{k+1}^{-} H_k^T [H_k P_{k+1}^{-} H_k^T + R_\mu]^{-1} \\ \hat{x}_{k+1}^{+} &= \hat{x}_{k+1}^{-} + K_{k+1}\left(y_k - \frac{1}{2}x_{k+1}^{-T} x_{k+1}^{-}\right) \\ P_{k+1}^{+} &= (I - K_{k+1} H_k) P_{k+1}^{-} \end{aligned}$$

here Hk is the linearization of the output measurement equation computed for x = xˆ − k+1, i.e., Hk = xˆ −T k+1. The covariance matrix of the process and measurement noises are assumed to be Rw = diag([0.1 0.1]) (where diag([a1 . . . an]) is a diagonal matrix whose diagonal entries starting in the upper left corner are a1, . . . , an) and Rµ = 5, respectively, while the EKF covariance matrix is initialized as P + 0 = diag([2 2]). In the first simulated scenario, the vehicle was commanded to execute a lawn-mowing maneuver (consisting of a succession of orthogonal line segments). The speed of the vehicle was kept constant and equal to 1 m/s along each segment, except when required to change orientation during the transition from one to the next segment; in the latter case, the vehicle was supposed to have the capability to rotate in place. Figure 5 shows the path followed by the vehicle and its position as estimated using the EKF; the figure also shows the ellipsoid corresponding to the EKF covariance matrix along the path.

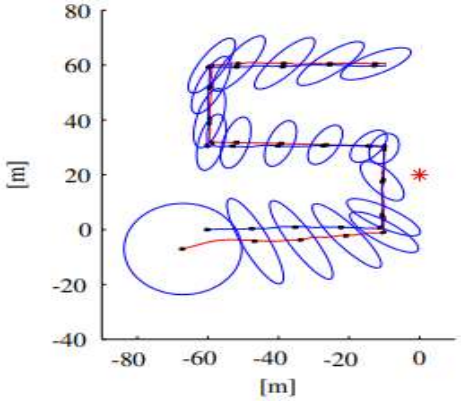

Figure 2. Real (blue) and estimated (red) path of a vehicle moving along orthogonal segments of a line using an Extended Kalman Filter (EKF) and range measurements from a single beacon in position [0, 20] m. The ellipses represent the covariance matrix of the EKF, while the red star represents the position of the transponder.

Figure 2 shows the time-evolution of different variables of interest: the norm of the estimation error, the distance of the vehicle from the transponder, the eigenvalues of the EKF covariance matrix and the observability index, C −1 . Notice that the lower eigenvalue of the EKF covariance matrix quickly decreases to a value related to the range measurement covariance; the higher eigenvalue, howeverexhibits more complicated dynamics

related to the AUV path and decreases when the observability index takes large values. The intervals where the observability index, C −1 , is equal to zero correspond to the rotation of the AUV in place, when it moves from one segment to the following.

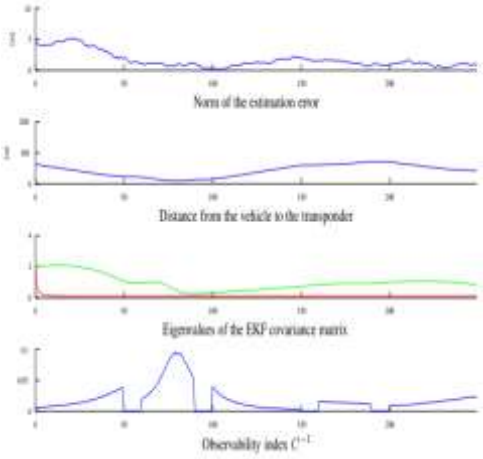

Figure 3. Variables of interest related to the paths in Figure 5: observability index C −1 , eigenvalues of the EKF covariance matrix, distance from the vehicle to the transponder and the norm of the estimation error.

We performed two sets of simulations with the vehicle driving around circumferences centered on the transponder to further illustrate the connection between the observability index and the filter's performance. The first round of simulations included driving the vehicle at varying speeds (0.5 m/s, 1 m/s, 1.5 m/s, and 2 m/s), which correspond to different values of the observability index (see Figure 7 for the pathways). Similar remarks apply to the higher eigenvalues of the EKF covariance matrix, as shown in Figure 8, indicating that the estimate error reduces more slowly along the route with a lower instantaneous observability index (solid line, conducted at the lowest speed).

In-Vehicle Tests

Experiments Here we report the outcomes of our attempts to put the observability index presented in this work to the test in a realistic setting. Beacon detection, which may be thought of as the inverse issue of single beacon localization discussed above, is the topic of this article. In this case, the vehicle already knows its location and must estimate the beacon's position using range measurements. The field experiments were conducted using an autonomous marine vehicle fitted with an acoustic range device that could determine its distance from an acoustic transponder anchored to the bottom at a known place. The trials were conducted in Lisbon, Portugal, in the Nations Park (the former location of Expo 98) (Lat: 38.766, Long: 9.03).

Construct for Experiment

For the sake of convenience, the tests were carried out using an ASV instead of a true AUV. This eliminated the need for time-consuming AUV localization testing, allowing the beacon detection system to be quickly put through its paces. In reality, a GNSS system may be used to determine the ASV's location if the proper configuration is used. However, from a practical acoustics perspective, it is comparable to the difficulty of AUV-based single beacon localization to perform ASV-based beacon detection using range measurements alone. Medusa, the ASV utilized in the trials, was created at the Instituto Superior T'ecnico of Lisbon's Laboratory of Robotics and Systems in Engineering and Science (LARSyS; see Figure 11). The vehicle's two side thrusters respond separately to controls for surge and yaw, allowing it a wide range of maneuverability. The vehicle has a Global Navigation Satellite System (GNSS) and an Attitude and Heading Reference System (AHRS), and it can talk to other devices on land through WiFi or to those underwater using an acoustic modem that doubles as a ranging unit (Tritech Micron Modem; see Figure 12 (right)). The transponder is simply a Tritech Modem unit (Figure 12 (left)) programmed to reply to inquiries from the surface modem, and it is placed at a known site underwater at 2 m depth. In response, the latter determines the distance between the surface and underwater units by calculating the round-trip travel time between them and applying the value of the speed of sound in water. The transponder was tethered to a surface support system via wire for charging and testing reasons.

Figure 5. The Medusa autonomous surface vessel.

Figure 6. Fixed transponder (left) and acoustic modem/ranging device on the Medusa nose cone (right).

Since the speed of sound in water is an integral part of calculating the distance between the ASV and the transponder, every effort was made to precisely measure it with a specialized instrument on a daily basis before the tests began. For the observability study, the ASV was instructed to follow either a series of circular paths centered on the transponder or a series of parallel/orthogonal segments (some of which were radial with respect to the transponder). All of the GNSS coordinates, compass headings, and range measurements made by the ASV were recorded and saved. An Extended Kalman Filter with equations similar to Equations (17)-(19) was applied to the processed data to assess its efficacy. The filter was developed with on-board ASV implementation in mind, so it handles temporary range measurement losses and updates the observer using only the velocity measurement (as in a conventional dead reckoning method) when no range information is available (a sample is taken every few seconds). Process and measurement noises are assumed to have covariance matrices Rw = diag([0.1 0.1]) and R = 5, whereas the EKF covariance matrix is initialized as P + 0 = diag([2 2]), as in the numerical simulation examples. To reiterate, the problem of estimating the position of the autonomous vehicle with respect to the transponder is conceptually and experimentally similar to the problem of estimating the position of the transponder (as if it were unknown) given that the position of the vehicle is known. The second case is the subject of the experiments detailed below. Results from Experiments Multiple experiments were conducted, and their data was analyzed to produce consistent findings. The first experiment included guiding the ASV along a series of parallel and orthogonal lines in a square area of roughly 100 by 100 meters. The ASV's flight plan is seen in Figure 13. The remote base station (Medusa Base) responsible for receiving and storing data from the ASV can be seen in the background, and the black squares represent the transponder's estimated position at various times during the mission.

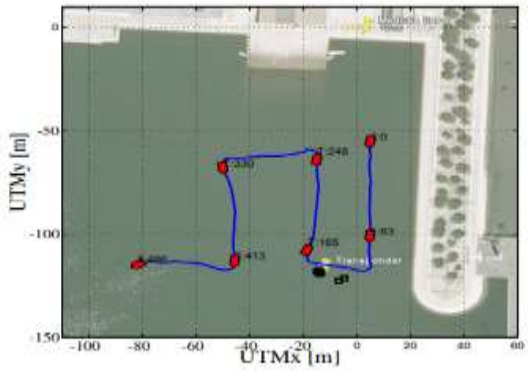

Figure 7. Path followed by the Medusa Autonomous Surface Vessel (ASV) during the first mission.

Information useful to the observability analysis may be shown in Figure 7. The top graph displays the calculated inverse of the condition number of the observability matrix in Equation (9) when genuine relative displacement is taken into account. The accurate location of the transponder and the GNSS readings of the ASV are used to calculate the true displacement, x, between the transponder and the ASV. The observer's estimate error is shown in Figure 14's second plot. The filter is set to estimate the transponder's position to be 10 meters from its actual location, in a circle centered on the ASV and having a radius equal to the range measurement. Figure 14's third figure compares the acoustic ranging device readings (blue) and GNSS readings (red) for the distance between the ASV and the transponder. It should be noted that the modem measurement is relatively precise, but that updates occur slowly and that there are occasional time frames with transient connection losses (this is to be anticipated, given the unfavorable circumstances of sonic propagation in extremely shallow seas). Figure 14's fourth panels provide the values of, sin(), and cos(2) (using Equation (12) as a reference), while the final graphs display the upper and lower eigenvalues of the EKF covariance matrix. Figures 13 and 14 show crucial parts of the mission that need to be highlighted right now. The filter error drops more rapidly while the ASV is approaching the transponder (within the time range of 80-180 s) than when it is receding from it. Also, keep in mind that both the EKF eigenvalues increase due to the process measurement noise covariance, while the filter error is kept low using dead-reckoning data in the absence of range measurements. In the second experiment, shown in Figure 15, the ASV was instructed to go in a circle around the transponder. As can be seen in Figure 16, the ASV maintains a constant and (and a similarly constant speed). In particular, the observability index is maximized at = 2. In contrast to the behavior seen in the previous mission, the filter estimation error drops rapidly and smoothly in this one, and the higher eigenvalue of the EKF covariance matrix stays confined throughout the experiment.

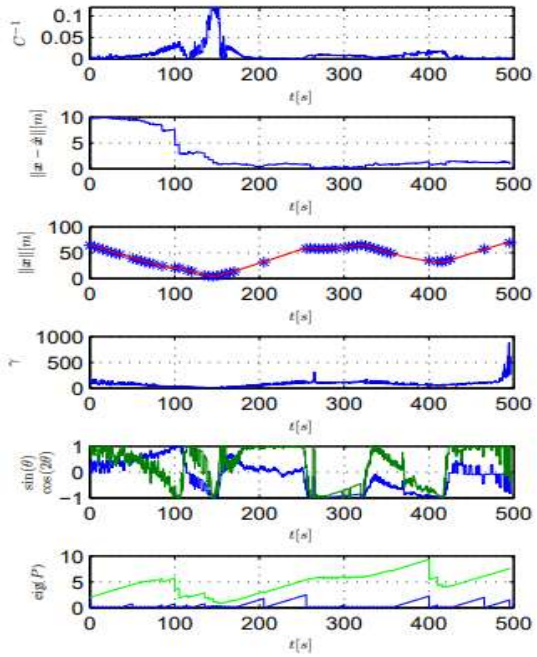

Figure 8. Observability parameters during the first mission: inverse of condition number (top plot), norm of estimation error (second plot from top), measurements of the range between the vehicle and the transponder (blue stars) and GNSS (red line) (third plot), γ (fourth plot), sin(θ) (blue) and cos(2θ) (green) (fifth plot) and eigenvalues of the EKF covariance matrix (last plot).

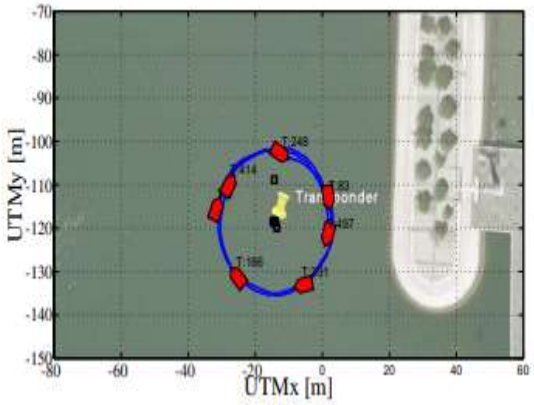

Figure 9. Path of the robot during the second mission.

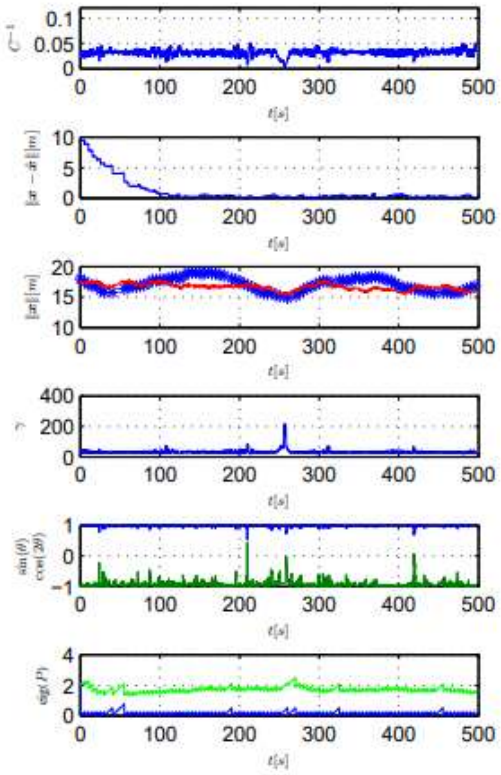

Figure 10. Observability parameters during the second mission: inverse of condition number (top plot), norm of estimation error (second plot from top), measurements of the range between the vehicle and the transponder (blue stars) and GNSS (red line) (third plot), γ (fourth plot), sin(θ) (blue) and cos(2θ) (green) (fifth plot) and eigenvalues of the EKF covariance matrix (last plot).

Finally, the ASV was programmed to travel along a sinusoidal path (shown in Figures 17 and 18), an example in which the observability index has a significant impact on the speed with which the estimation error decreases and the bounds within which the EKF covariance eigenvalues matrix can be calculated. In the experiment's final phase, range measurements are received in a dispersed fashion, and the increase in EKF eigenvalues due to the AUV process noise covariance can be observed. The attached multimedia file depicts a reconstruction, using experimental data, of the observability metric analysis in relation to the previously provided case studies. Animations showing ASV movement, EKF filter effectiveness, and observability index variability across many case studies are shown in the film.

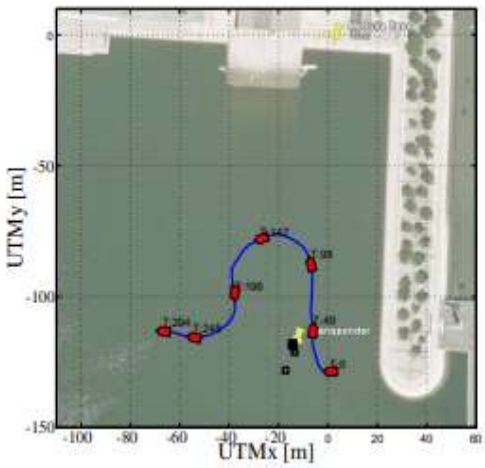

Figure 11. Path of the robot during the third mission.

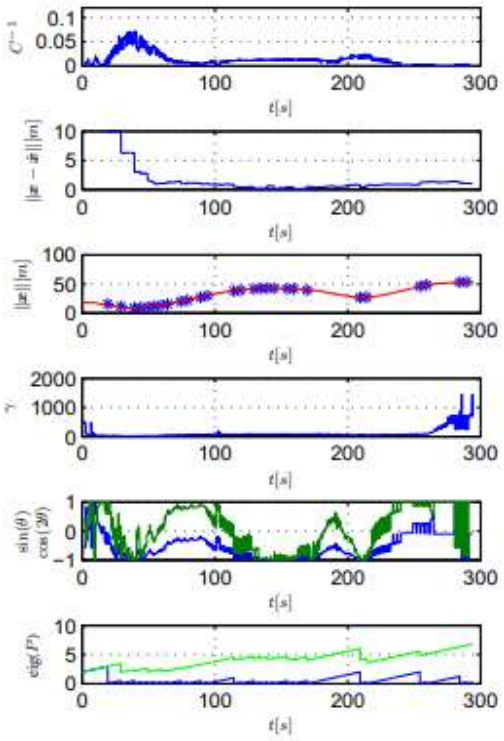

Figure 12. Observability parameters during the third mission: inverse of condition number (top plot), norm of estimation error (second plot from top), measurements of the range between the vehicle and the transponder (blue stars) and GNSS (red line) (third plot), γ (fourth plot), sin(θ) (blue) and cos(2θ) (green) (fifth plot) and eigenvalues of the EKF covariance matrix (last plot)

Conclusion

In this study, we looked at the structural observability aspects of two distinct localization problems: localizing a single beacon and estimating the relative location of two AUVs using just range data. The observability of vehicle movements was quantified using a suggested metric that made use of nonlinear observability ideas. The suggested measure was shown successful via simulation analysis and experimental verification. The ideal real-time trajectory planning algorithms that take use of the accepted metric will be developed, and the study of various kinds of observers will be the focus of future research. We will also discuss how to generalize these concepts to the scenario of several vehicles.

References

[1].Larsen, M. Synthetic Long Baseline Navigation of Underwater Vehicles. In Proceedings of MTS/IEEE Conference Oceans 2000, Providence, RI, USA, 11–14 September 2000; pp. 2043–2050.

[2]. Gadre, A.; Stilwell, D. Underwater Navigation in the Presence of Unknown Currents Based on Range Measurements from a Single Location. In Proceedings 2005 American Control Conference, Portland, USA, 8–10 June 2005; pp. 565–661.

[3]. Bahr, A.; Leonard, J.; Fallon, M. Cooperative localization for autonomous underwater vehicles. Int. J. Robot. Res. 2009, 28, 714–728.

[4]. Webster, S.; Eustice, R.; Singh, H.; Whitcomb, L. Preliminary Deep Water Results in Single-Beacon One-Way-Travel-Time Acoustic Navigation for Underwater Vehicles. In Proceedings of 2009 IEEE/RSJ International Conference on Intelligent Robots and Systems, St. Louis, MO, USA, 10–15 October 2009; pp. 2053–2060.

[5]. Hartsfield, J. Single Transponder Range Only Navigation Geometry (STRONG) Applied to REMUS Autonomous Underwater Vehicles. Ph.D. Thesis, Massachusetts Institute of Technology and Woods Hole Oceanographic Institution, Cambridge, MA, USA, August 2005.

[6]. Gadre, A. Observability Analysis in Navigation Systems with an Underwater Vehicle Application. Ph.D. Thesis, Virginia Polytechnic Institute and State University, Blacksburg, VA, USA, 2007.

[7]. Ross, A.; Jouffroy, J. Remarks on the Observability of Single Beacon Underwater Navigation. In Proceedings International Symposium on Unmanned Untethered Submersible Technology, Durham, NH, USA, August 2005.

[8]. Jouffroy, J.; Reger, J. An Algebraic Perspective to Single-Transponder Underwater Navigation. In Proceedings of IEEE International Conference on Control Applications, IEEE International Symposium on Computer-Aided Control Systems Design, IEEE International Symposium on Intelligent Control, Munich, Germany, 4–6 October 2006; pp. 1789–1794.

[9]. Bahr, A. Cooperative Localization for Autonomous Underwater Vehicles. Ph.D. Thesis, Massachusetts Institute of Technology and Woods Hole Oceanographic Institution, Cambridge, MA, USA, February 2008.

[10]. Fallon, M.; Papadopoulos, G.; Leonard, J.; Patrikalakis, N. Cooperative AUV Navigation using a single maneuvering surface craft. Int.J. Robot. Res. 2010, 29, 1461–1474.

[11]. Singh, S.; Grund, M.; Bingham, B.; Eustice, R.; Singh, H.; Freitag, L. Underwater Acoustic Navigation with the WHOI Micro-Modem. In Proceedings of MTS/IEEE Conference and Exhibition OCEANS 2000, Providence, RI, USA, 18–21 September 2000; pp. 1–4.

[12]. Papadopoulos, G.; Fallon, M.; Leonard, J.; Patrikalakis, N. Cooperative Localization of Marine Vehicles Using Nonlinear State Estimation. In Proceedings of 2010 IEEE/RSJ International Conference on Intelligent Robots and Systems, Taipei, Taiwan, 18–22 October 2010; pp. 4874–4879.

[13]. Hong, S.; Chun, H.; Kwon, S.; Lee, M. Observability measures and their application to GPS/INS. IEEE Trans. Veh. Technol. 2008, 57, 97–106.

[14]. Sa´ude, J.; Aguiar, A. Single Beacon Acoustic Navigation for an AUV in the Presence of Unknown Ocean Currents. In Proceedings of 8th IFAC Conference on Manoeuvring and Control of Marine Craft, Guaruja (SP), Brazil, 16–18 September 2009; pp. 298–303.

[15]. Batista, P.; Silvestre, C.; Oliveira, P. Single range aided navigation and source localization: Observability and filter design. Syst. Control Lett. 2011, 60, 665–673.

[16]. Casalino, G.; Caiti, A.; Turetta, A.; Simetti, E. RT2 : Real-time ray-tracing for underwater range evaluation. Intell. Serv. Robot. 2011, 4, 259–270.

[17]. Parlangeli, G.; Pedone, P.; Indiveri, G. Relative Pose Observability Analysis for 3D Nonholonomic Vehicles Based on Range Measurements Only. In Proceedings of 9th IFAC Conference on Manoeuvring and Control of Marine Craft, Arenzano (GE), Italy, 19–21 September 2012.

[18]. Chen, B.; Hu, J.; Li, H.; Sun, Z. Measure Observability by the Generalized Informational Correlation. In Proceedings of 46th IEEE Conference on Decision and Control, New Orleans, LA, USA, 12–14 December 2007; pp. 5570–5574.

[19]. Jauffret, C. Observability and Fisher information matrix in nonlinear regression. IEEE Trans. Aerosp. Electron. Syst. 2007, 43, 756–759.

[20]. Grossman, W. Bearings-Only Tracking: A Hybrid Coordinate System Approach. In Proceedings of the 30th IEEE Conference on Decision and Control, Brighton, UK, December 1991; pp. 2032–2037.